

Sodium triple quantum MR signal extraction using a single-pulse sequence with single quantum time efficiency

Simon Reichert^{1,2,3}  | Victor Schepkin⁴  | Dennis Kleimaier¹ | Frank G. Zöllner^{1,2,3}  | Lothar R. Schad^{1,2}

¹ Computer Assisted Clinical Medicine, Medical Faculty Mannheim, Heidelberg University, Mannheim, Germany

² Mannheim Institute for Intelligent Systems in Medicine, Medical Faculty Mannheim, Heidelberg University, Mannheim, Germany

³ Cooperative Core Facility Animal Scanner ZI, Medical Faculty Mannheim, Heidelberg University, Mannheim, Germany

⁴ National High Magnetic Field Laboratory, Florida State University, Tallahassee, Florida, USA

Correspondence

Simon Reichert, Computer Assisted Clinical Medicine, Medical Faculty Mannheim, Heidelberg University, Mannheim, Germany.

Email:

simon.reichert@medma.uni-heidelberg.de

Funding information

State of Florida; German Research Foundation, Grant/Award Number: 410981386; National High Magnetic Field Laboratory; National Science Foundation, Grant/Award Number: DMR-1644779

Abstract

Purpose: Sodium triple quantum (TQ) signal has been shown to be a valuable biomarker for cell viability. Despite its clinical potential, application of Sodium TQ signal is hindered by complex pulse sequences with long scan times. This study proposes a method to approximate the TQ signal using a single excitation pulse without phase cycling.

Methods: The proposed method is based on a single excitation pulse and a comparison of the free induction decay (FID) with the integral of the FID combined with a shifting reconstruction window. The TQ signal is calculated from this FID only. As a proof of concept, the method was also combined with a multi-echo UTE imaging sequence on a 9.4 T preclinical MRI scanner for the possibility of fast TQ MRI.

Results: The extracted Sodium TQ signals of single-pulse and spin echo FIDs were in close agreement with theory and TQ measurement by traditional three-pulse sequence (TQ time proportional phase increment [TQTPPI]). For 2%, 4%, and 6% agar samples, the absolute deviations of the maximum TQ signals between SE and theoretical (time proportional phase increment TQTPPI) TQ signals were less than 1.2% (2.4%), and relative deviations were less than 4.6% (6.8%). The impact of multi-compartment systems and noise on the accuracy of the TQ signal was small for simulated data. The systematic error was <3.4% for a single quantum (SQ) SNR of 5 and at maximum <2.5% for a multi-compartment system. The method also showed the potential of fast in vivo SQ and TQ imaging.

Conclusion: Simultaneous SQ and TQ MRI using only a single-pulse sequence and SQ time efficiency has been demonstrated. This may leverage the full potential of the Sodium TQ signal in clinical applications.

KEYWORDS

Sodium MRI, sodium triple quantum coherences, multiple quantum coherences, SodiumTQ, multi-quantum

1 | INTRODUCTION

The Sodium nucleus has attractive NMR and MRI properties both from physical and a biomedical perspective.^{1,2}

Sodium ions play a vital role in several transport processes across the cell membrane as well as electric signaling between neurons.³ For example, the sodium-potassium pump maintains a large concentration gradient between the intracellular and extracellular space by continuously removing Sodium ions from the cell.^{4,5} This pumping process consumes up to two-thirds of the cellular energy. Hence, a breakdown of the energy supply results in a failure of the sodium-potassium pump and thus an influx of Sodium ions into the cell. Alterations in the intracellular sodium concentration are linked to several other vital cellular processes and consequently reflect early pathophysiological changes.²

The ²³Na nucleus has a spin of 3/2; therefore, the Sodium electrical quadrupole moment interacts with surrounding electric field gradients created by the molecular environment.^{3,6} In the case of a slowly fluctuating electric field gradient, as for instance during ion interactions with proteins and other macromolecules, these electric quadrupole interactions cause biexponential relaxation and allow the formation of triple quantum (TQ) coherences subsequent to the single quantum (SQ) coherence.^{3,7-11} The weighted mean value of the intra- and extracellular Sodium concentrations, the tissue sodium concentration (TSC), can be determined from the sodium SQ signal to gain valuable noninvasive information about cell viability and physiology.^{1-3,12,13} However, the SQ signal does not allow the differentiation between increased intracellular sodium concentration and increased extracellular volume.¹⁴ On the other hand, the TQ signal has been shown to have a higher weighting toward the intracellular sodium content than the SQ signal.¹⁵⁻²² Both sodium signals are potential valuable biomarkers for cell viability.²³⁻²⁸ A combined measurement of SQ and TQ signals²⁹⁻³¹ might provide more insights into cellular processes. Several studies with perfused rat heart systems,^{15,19,20,32-34} brain ischemia,³⁵ and tumors^{36,37} and in vitro experiments using an MR-compatible bioreactor systems³⁸⁻⁴¹ have demonstrated a correlation of the TQ signal with cell viability. The TQ signal increases with the intracellular sodium concentration²⁰ and depends on the sodium^{15,20} and protein^{15,19} concentrations as well as the folding state of proteins.⁴² Thus, the TQ signal increases the value of sodium MRI as a valuable biomarker for cell viability.^{15,16,19,32,33,35,39,41}

Because the TQ signal is detected indirectly,⁷ complicated phase cycling multi-pulse sequences are used.^{6,43-46} The typical TQ filtering (TQF) sequence uses three RF

pulses and two evolution periods between the pulses with an optional 180° refocusing pulse during the first evolution period.³ These sequences exploit the fact that the TQ coherences accumulate phase three times faster than the SQ signal. Therefore, phase alterations in the pulse sequence provide a tool for selection of the desired TQ signal. The first 90° RF pulse creates T_{11} coherences that are converted to T_{31} coherences during the first evolution period τ_{evo} . The second 90° pulse transforms the T_{31} coherences to T_{33} coherences, which accumulate a three times larger phase shift than SQ signal. The mixing time τ_{mix} is usually selected to be as short as possible to avoid MR signal decay (Figure 1). At the end, a third 90° RF pulse transforms the T_{33} coherences back to T_{31} , which later evolve into observable T_{11} MR signal. The phases of all three RF pulses are incremented in every scan, and the signals are summed or processed independently. The conventional TQF sequence chooses the phase increment in such a way that only the TQ signal passes the above filter. Modifications of the conventional phase cycle help to reduce the impact of B_1 and B_0 inhomogeneities^{29,47-49} or filter out unwanted echoes.^{29,30,49} Another way to detect TQ signal is the time proportional phase increment (TQTPPI) sequence.^{6,50} This sequence is very similar to the TQF sequence as described above, with the evolution time being additionally incremented in every phase step. The TQTPPI sequence simultaneously detects both the SQ and TQ signals at distinct frequencies and therefore simplifies the TQ signal quantification by normalizing it to the SQ signal.⁶

The Indicated requirement of a phase cycling scheme combined with multiple RF pulses results in a long scan time and a large specific absorption rate. Furthermore, T_{33} coherences are prone to B_0 and B_1^+ inhomogeneities. B_0 inhomogeneities have a three times larger effect on T_{33} state than on SQ coherences. The TQ signal has a $\sin^5\theta$ dependency on the RF flip angle θ .⁵¹ These drawbacks and the low SNR of the TQ filtered signal currently hinder a clinical application of the TQ signal.

However, the evolution of the T_{31} coherences after the first RF pulse already encode the relevant TQ state information about the molecular environment of the sodium nuclei.^{3,10,11} The other parts of the conventional TQ pulse sequences have the sole purpose of making the creation of the T_{31} state detectable. Direct extraction of T_{31} coherences have a huge potential to simplify and accelerate the detection of TQ signals. Based on this idea, this study presents a novel method to extract the TQ signal using only free induction decay (FID) from a single-pulse (SP) sequence or a spin-echo (SE) sequence. We compare such TQ signal with theory and the TQ signal from the state-of-the-art TQTPPI sequence in agarose as a tissue

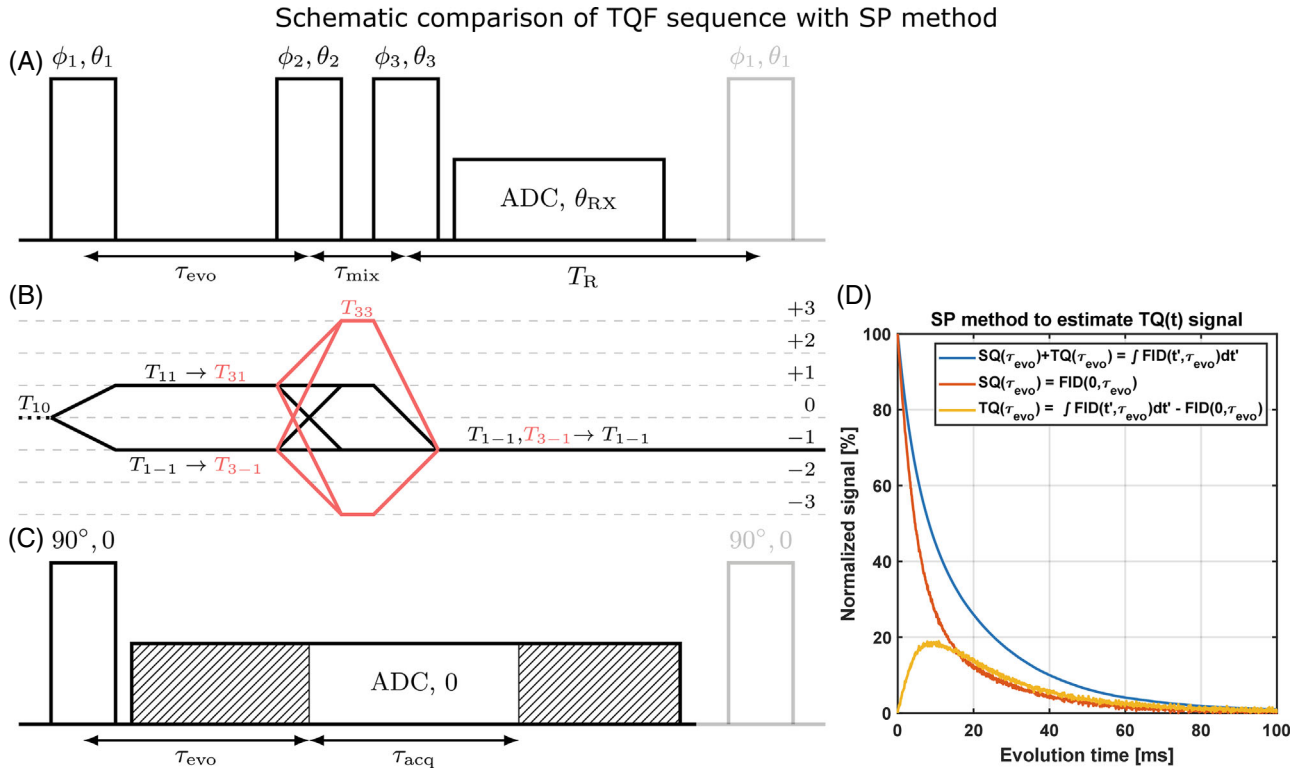


FIGURE 1 (A) Exemplary conventional TQ pulse sequence. The T_{31} coherences are created after the first 90° pulse during τ_{evo} . The rest of the pulse sequence is only necessary to extract TQ signal from the T_{31} state by observing oscillations of the final T_{11} signal. (B) Coherence pathways for the TQ pulse sequence. (C) In this study, the three-pulse TQ sequence was replaced by a single-pulse sequence with a prolonged acquisition window. Shifting the processing window across the total acquisition data yields the signal for a set of different τ_{evo} . The shaded area indicates the points removed from the FID for the specific evolution time τ_{evo} . (D) The difference of the integration of the whole FID and the SQ spectrum for each τ_{evo} represents the TQ signal. FID, free induction decay; SQ, single quantum; TQ, triple quantum.

model system. We investigate the performance of our method in multi-compartment systems and in the presence of noise using simulated data. As a proof-of-concept, we also combine this method with a multi-echo radial UTE sequence to demonstrate the possibility of fast sodium MR imaging in vitro.

2 | METHODS

2.1 | The SP method

The density operator σ describing the sodium nuclei spin system can be expressed in irreducible spherical tensor operators (ISTO)^{52,53} basis

$$\sigma = \sum_{mn} A_{mn} T_{mn},$$

where A_{mn} are the amplitudes of the irreducible spherical tensor operators basis elements T_{mn} and $m = 1, 2, 3$ and $n = -3, \dots, 3$ are the coherence rank and order, respectively. We further use the substitutions $A_{\text{SQ}} = A_{11}$ and $A_{\text{TQ}} = A_{31}$ to clarify the meaning of the respective amplitudes.

Immediately after the 90° excitation RF pulse, the MR signal completely consists of T_{11} coherences. We only consider the isotropic case as an approximation for biological tissue, despite a small double quantum (DQ) signal, that was measured in muscle tissue⁵⁴ and the brain.^{55,56} The coherences evolve according to the evolution equation^{10,11}

$$\begin{pmatrix} A_{\text{SQ}} \\ A_{\text{TQ}} \end{pmatrix} \rightarrow \begin{pmatrix} f_{11}^{(1)}(t) & f_{13}^{(1)}(t) \\ f_{31}^{(1)}(t) & f_{33}^{(1)}(t) \end{pmatrix} \cdot \begin{pmatrix} A_{\text{SQ}} \\ A_{\text{TQ}} \end{pmatrix}, \quad (1)$$

where

$$f_{11}^{(1)}(t) = 0.4 \exp\left(-\frac{t}{T_{2s}}\right) + 0.6 \exp\left(-\frac{t}{T_{2f}}\right), \quad (2)$$

$$f_{13}^{(1)}(t) = f_{31}^{(1)}(t) = \frac{\sqrt{6}}{5} \left(\exp\left(-\frac{t}{T_{2f}}\right) - \exp\left(-\frac{t}{T_{2s}}\right) \right), \quad (3)$$

and

$$f_{33}^{(1)}(t) = 0.6 \exp\left(-\frac{t}{T_{2s}}\right) + 0.4 \exp\left(-\frac{t}{T_{2f}}\right) \quad (4)$$

are the evolution functions for the transitions $T_{11} \rightarrow T_{11}$ and $T_{31} \rightarrow T_{11}$ with the fast and slow relaxation times T_{2f} and T_{2s} , respectively. After the evolution period τ_{evo} , the amplitude of the T_{11} coherence is $A_{\text{SQ}} = f_{11}^{(1)}(\tau_{\text{evo}})$ and the T_{31} amplitude is $A_{\text{TQ}} = f_{31}^{(1)}(\tau_{\text{evo}})$. The amplitude A_{TQ} and the relaxation times encode information about the molecular environment of the sodium nucleus.

However, the T_{31} coherences are invisible to the receiver coil; therefore, it is impossible to directly detect them.⁷ Thus, the T_{31} coherences must be converted back to the detectable T_{11} coherences. The conventional TQF sequence applies a second and third 90° RF pulse to transfer the T_{31} coherences to T_{33} coherences and back combined with phase cycling as shown in Figure 1A.

Our aim was to reduce the complexity of the TQ pulse sequence, while still being able to extract the TQ signal. In contrast to the TQF approach, which measures the transition $T_{11} \rightarrow T_{31} \rightarrow T_{33} \rightarrow T_{31} \rightarrow T_{11}$, our method measures only the transition $T_{11} \rightarrow T_{31} \rightarrow T_{11}$. The following introduces our method step-by-step.

First, the FID after a single-pulse and evolution period of τ_{evo} is described by:

$$\text{FID}(t, \tau_{\text{evo}}) = A_{\text{SQ}}(\tau_{\text{evo}})f_{11}^{(1)}(t) + A_{\text{TQ}}(\tau_{\text{evo}})f_{13}^{(1)}(t). \quad (5)$$

The second term on the right side represents the evolution of the T_{31} coherences that evolved during the first evolution period (amplitude $A_{\text{TQ}}(\tau_{\text{evo}})$) from the detectable T_{11} coherences.

Secondly, for extraction of A_{SQ} and A_{TQ} , we exploit the fact that the integral of a Lorentzian function, that is, the real part of the Fourier transform (FT) of a one-sided decaying exponential function, is independent of the width, that is, relaxation time $T_2^{(*)}$:

$$\int_{-\infty}^{+\infty} \frac{T_2}{1 + T_2^2 \omega^2} d\omega = \pi. \quad (6)$$

The TQ signal, that is, $f_{31}^{(1)}(\tau_{\text{evo}})$, consists of a difference between two exponential functions and therefore the integral over its FT vanishes. On the other hand, the integral over the FT of the SQ signal part is proportional to its amplitude A_{SQ} . In contrast, the integral over the FID contains both signals. The TQ signal then can be extracted by subtraction of both normalized integrals for every τ_{evo} -step

$$\begin{aligned} & A_{\text{TQ}}(\tau_{\text{evo}}) \\ &= \text{Norm} \cdot \left(\frac{\int \text{FID}(t, \tau_{\text{evo}}) dt}{\int \text{FID}(t, 0) dt} - \frac{\int \text{FT}(\text{FID}(t, \tau_{\text{evo}})) d\omega}{\int \text{FT}(\text{FID}(t, 0)) d\omega} \right) \\ &= \text{Norm} \cdot \left(\frac{\int \text{FID}(t, \tau_{\text{evo}}) dt}{\int \text{FID}(t, 0) dt} - \frac{\text{FID}(0, \tau_{\text{evo}})}{\text{FID}(0, 0)} \right). \end{aligned} \quad (7)$$

The full calculation can be found in the Supporting Information, which also demonstrates the necessity of a correction factor with respect to $f_{13}^{(1)}(t)$ from Equation (3):

$$\text{Norm} = \frac{\int f_{11}^{(1)}(t) dt}{\int f_{13}^{(1)}(t) dt} = \frac{A_s T_{2s} + A_f T_{2f}}{\frac{\sqrt{6}}{5} (T_{2s} - T_{2f})}. \quad (8)$$

Lastly, in contrast to the conventional TQF/TQTPPI pulse sequence, an extended acquisition window can be used to retrieve results of many evolution times from the same measurement. As illustrated in Figure 1C), the acquisition window starts directly after the excitation pulse instead of waiting for a certain evolution duration τ_{evo} . If τ_{acq} is the desired acquisition time, then for a specific evolution time τ_{evo} , only the FID points between $[\tau_{\text{evo}}, \tau_{\text{evo}} + \tau_{\text{acq}}]$ are used. Thus, the desired acquisition time is shifted across the extended acquisition window to extract the effect of the evolution time on the TQ signal. A short sample application of this method can be found at https://github.com/Computer-Assisted-Clinical-Medicine/Singlepulse_-TQ_Code.

Note that the method can be applied to any equidistantly sampled FID, independent of the sampling method of the FID. Hence, this method is also applicable to imaging using for example a multi-echo sequence. However, if the FID is not equidistantly sampled, either the integral must be adapted by considering the τ_{evo} step-width or the missing points need to be interpolated.

2.2 | Simulations

For multi-compartment systems (MCS), which yield a more accurate description for biological tissue, the integrals in (7) become more complicated. To investigate the validity of the proposed method in such environments, we consider the case of a two-compartment system with two biexponential compartments. The corresponding FID and theoretical TQ signal are

$$\text{FID}_{\text{MCS}}(t) = (1 - c_{\text{ex}})\text{FID}_{\text{in}}(t) + c_{\text{ex}}\text{FID}_{\text{ex}}(t), \quad (9)$$

$$\text{TQ}_{\text{exp}}(t) = (1 - c_{\text{ex}})\text{TQ}_{\text{in}}(t) + c_{\text{ex}}\text{TQ}_{\text{ex}}(t), \quad (10)$$

Where $\text{FID}_{\text{in}}(t)$, $\text{FID}_{\text{ex}}(t)$, $\text{TQ}_{\text{in}}(t)$, and $\text{TQ}_{\text{ex}}(t)$ are the FID and TQ signals that correspond to the model intra- and extracellular compartment, respectively, and c_{ex} is the contribution of the extracellular compartment. It has been previously shown that both the extra- and intracellular compartments yield a TQ signal⁵⁷⁻⁶² and biexponential relaxation.¹⁵⁻²² For quantitative evaluation of

such case, the T_2 relaxation times of 2% agar (“extracellular”, $T_{2s} = 44$ ms, $T_{2f} = 9$ ms) and 6% agar (“intracellular”, $T_{2s} = 32$ ms, $T_{2f} = 3.7$ ms) were used to model the two-compartment system with two biexponential compartments.^{15–22}

The value of c_{ex} was varied in the range from 0 to 1, and FIDs were generated according to Equation (9). The SP TQ method was applied to the FID to extract the TQ signal. The results were compared to the expected TQ signal calculated by Equation (10).

To investigate the impact of noise on the TQ quantification using the SP method, we simulated FIDs in a single compartment system according to Equation (5) and added Gaussian white noise to the signal. The output of the SP method was evaluated for different noise levels corresponding to a SNR of the SQ signal of 50, 20, 10, and 5. Additionally, the same noise was subtracted from the TQ signal after applying the SP method to isolate the error of the SP method on the TQ signal, which is buried under noise for lower SNR values.

2.3 | Experimental

Measurements were performed at a 9.4 T preclinical MRI scanner (Biospec 94/20, Bruker, Ettlingen, Germany) using a linear polarized $^1\text{H}/\text{sodium}$ Bruker volume coil. Inner diameter was 72 mm with a length of 100 mm for the sodium channel.

The samples consisted of [0, 2, 4, 6] % w/w agarose with 154 mM NaCl, where the 0% agarose sample is just saline solution with 154 mM NaCl. Chemicals were purchased from Carl Roth GmbH (Karlsruhe, Germany). The solution was filled into 20 ml syringes (10 ml solution, diameter: 20 mm, length of the solution in the syringe: 35 mm) to avoid direct air contact and reduce B_0 inhomogeneity. For MR imaging, all agar samples were combined in a single phantom.

The standard Bruker SP sequence was used to measure sodium FIDs ($\omega_0 = 105.9$ MHz) with the following sequence parameters: flip angle 90° , repetition time $T_R = 500$ ms, number of averages $N_A = 64$, number of FID points $N_{fid} = 4096$, length of acquisition window $t_{acq} = 410$ ms, and a dwell time of $100 \mu\text{s}$. The pre-acquisition delay was $50 \mu\text{s}$. The number of τ_{evo} points was set to 2048 with $\tau_{evo,max} = 205$ ms. Total acquisition time of the single-pulse sequence was 32 s per sample. The FID was preprocessed as described in the Supporting Information section “Preprocessing of the SP FID”.

To determine the validity and accuracy of our method, the results were compared with theoretical predictions of the TQ signal and the results from TQTPPI sequence. The shapes of the TQ, SQ evolution curves, and the quantitative

values of the TQ signal maxima were used for analysis. The TQ signal maxima represents the mean over 10 points around maximum value to minimize the impact of single outliers. For the TQTPPI sequence, we fitted the TQ signal with the function $TQ(t) = A_{TQ} \left(\exp\left(-\frac{t}{T_{2s}}\right) - \exp\left(-\frac{t}{T_{2f}}\right) \right)$ and subtracted it from the signal to obtain an approximation of the noise level. The SD of this noise level defines the uncertainty of the TQTPPI TQ signal maximum.

Theoretical behavior of the TQ signal is determined by the transfer functions $f_{31}^{(1)}(\tau_{evo})$. The necessary T_2^* relaxation times for the sample were determined by a biexponential fit of the FID:

$$Y(t) = A_{SQ,1} \cdot \exp\left(-\frac{t}{T_{2s}}\right) + A_{SQ,2} \cdot \exp\left(-\frac{t}{T_{2f}}\right) + c, \quad (11)$$

where $Y(t)$ is the SP FID and c is a D.C. offset. The 0% Agar sample FID was fitted with a mono-exponential function

$$Y(t) = A_{SQ} \cdot \exp\left(-\frac{t}{T_2}\right) + c. \quad (12)$$

The TQTPPI relaxation times were determined in the same way.

For the TQTPPI measurements, we used a set of fixed- τ_{evo} TQTPPI sequence^{6,40} measurements with a 180° refocusing pulse at 26 different τ_{evo} times in the range of 0.4 to 200 ms. The repetition time TR was 400 ms, the number of phase cycles was 16 with 8 phase steps, and the number of averages NA was 4. Total acquisition time for each sample was in the range of 3 h. We used the sequence with the 180° refocusing pulse because the sequence without the 180° pulse resulted in additional stimulated echoes in the signal, see Supporting Information (section “Comparison of SP method with TQTPPI sequence wo/ 180° refocusing pulse”) for further information.^{29,30,49} The resulting FID decayed neither with the T_2 nor the T_2^* relaxation times, which complicates the comparison between both sequences.

For a better comparison of our method with the TQTPPI sequence signal, which decays with the T_2 instead of the T_2^* relaxation times, we sampled the T_2 FID with a SE sequence followed by application of our method. For the SE sequence, 256 echoes were equidistantly sampled with a minimum TE of 0.137 ms and an echo spacing of 0.78 ms. The length of the FID was doubled using zero filling at the end. The maximum TE was 300 ms, $T_R = 500$ ms, number of averages $N_A = 16$. Total scan time for each sample was 45 min. The SE FID was created by the maximum values of the echoes for each TE. The FIDs were corrected using the inverse of the corrected factor in Equation (8) with the T_2 relaxation times. The correction factor of the TQTPPI sequence uses the T_2^* relaxation times since the

first dimension FIDs decay with the T_2^* relaxation times as determined with Equations (11) and (12). To ensure a fair comparison, we also calculated the theoretical prediction using Equations (2) and (3) and the T_2 relaxation times obtained from a fit of the SE FID with fit Equation (12) for the 0% agar sample and Equation (11) for the 2%, 4%, and 6% agar samples.

For sodium MR imaging, a multi-echo version of the UTE sequence⁶³ was used with 64 echoes, a minimum TE of 0.09 ms, and an echo spacing of 3.78 ms. The length of the FIDs was doubled by zero filling at the end. Other imaging parameters were $T_R = 300$ ms, number of averages $N_A = 4$, $FOV = 68 \times 68 \times 68$ mm³, imaging matrix = $32 \times 32 \times 32$, spatial resolution of $2.125 \times 2.125 \times 2.125$ mm³, 3176 projections, a receiver bandwidth of 5 kHz, and a total acquisition duration of 1 h 3 min. To suppress noise from voxels outside the samples, we set voxels with <50% of the overall maximum value in the SQ image to 0. This method works well for simple phantoms, but for in vivo measurements more sophisticated methods like region growing, more sophisticated magnitude thresholding, or manual segmentation are used as a standard process.^{64–66} The SQ and TQ image were acquired simultaneously with the SQ scan time. From every echo, we created an SQ image, and the stack of SQ images yielded an FID for every voxel. For the reconstruction of the TQ image, we applied the SP TQ method described in this study voxelwise using Equation (7). The result was a TQ(t) evolution for every voxel. From this, a max(TQ) image was created that showed the maximum TQ values for each voxel. The sum(TQ) image was calculated by $\sum_i TQ(t_i) / \sum_i SQ(t_i)$. We also calculated the mean TQ signal for each sample over an exemplary slice. The uncertainty of the values was determined by the SD of all voxels.

3 | RESULTS

3.1 | Comparison of the SP TQ signal with theory and TQTPPI sequence

A comparison of the TQ signal determined by the SP method and the theoretical transfer functions $f_{13}^{(1)}(\tau_{\text{evo}})$ for all samples is presented in Figure 2. Relaxation times for $f_{13}^{(1)}(\tau_{\text{evo}})$ were determined by a biexponential fit of the single-pulse FID as summarized in Table 1. For the 2%, 4%, and 6% agar samples, the maximum TQ signals and the shape of the TQ signal relaxation of the SP method were in close agreement with the theoretical curve with a maximum relative deviation of the TQ maxima of <2%. For a quantitative comparison, the maximum TQ signals are summarized in Table 2. The single-pulse and

theoretical FIDs, that is, the corrected $f_{13}^{(1)}(\tau_{\text{evo}})$ curves using Equation (8), had the same relaxation times by design. However, the amplitudes of the experimental FIDs deviated from the theoretical values of 0.6 for the fast and 0.4 for the slow component, especially for the 4% agar sample. The extracted TQ signal for the 0% agar sample was non-zero for the SP method despite the theoretically expected zero TQ signal and a mono-exponential T_2 relaxation. In this case, the shape of the TQ evolution also strongly deviated from the expected build-up behavior.

Figure 3 compares the SP method with the TQTPPI pulse sequence. For both methods, the maxima of the TQ evolution curves approximately coincided for the 2%, 4%, 6% agar samples with a maximum relative deviation of the TQ maxima of <10%. For the 0% agar sample, the TQTPPI TQ signal was approximately zero, whereas in the SP method the TQ signal was non-vanishing. The relaxation times of both the SQ and TQ signals deviated substantially as the SP FID decayed with the T_2^* relaxation times, whereas the TQTPPI FID decayed with the T_2 relaxation times. The maximum TQ values and relaxation times for all samples and methods are summarized in Tables 1 and 2.

Figure 4 compares the TQ signal determined with the SE FID, TQTPPI sequence, and theoretical prediction. For all samples, including the 0% agar sample, the SE and TQTPPI TQ signals were in close agreement with each other and the theoretical prediction with a maximum relative deviation of the SE TQ maxima of <5% from the theoretical prediction and <7% for the TQTPPI TQ signal (excluding the 0% sample because division by 0). Furthermore, as shown in Table 1, the maximum TQ values were in close agreement except for the 4% agar sample, where the SE maximum TQ signal was larger than for the other two methods. This was caused by a peak close to the maximum of the TQ curve resulting from noise or a small artifact.

3.2 | Simulations

For estimation of the accuracy of the proposed SP method, a two-compartment model was investigated using relaxation times from our results of the 2% and the 6% agar samples. We varied the size of the compartments, c_{ex} , in the range of 0 to 1. Figure 5 shows a comparison of the theoretically expected TQ signal with the TQ signal determined by the SP method for both models with varying values of c_{ex} . Furthermore, the FID and TQ signal are shown for the c_{ex} parameter with the strongest deviation between the SP TQ signal and the expected TQ signal ($c_{\text{ex}} = 0.67$). The theoretically expected TQ signal was determined by

Comparison of SP method with theory

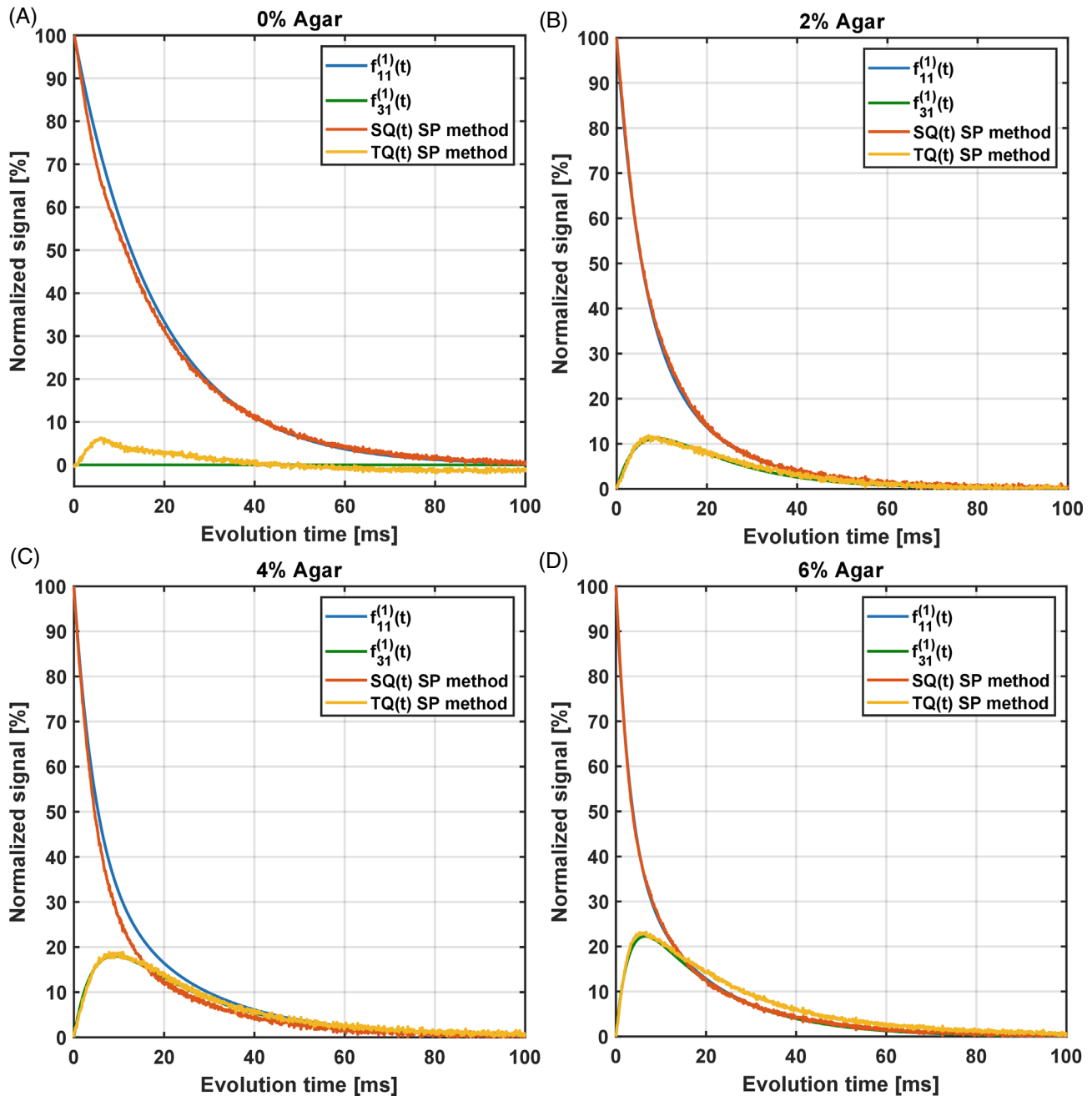


FIGURE 2 Comparison of the TQ signal from SP method and the theoretical transfer function $f_{31}^{(1)}(\tau_{\text{evo}})$ (corrected with Equation (8)) for (A) 0%, (B) 2%, (C) 4%, and (D) 6% agar samples. The relaxation times for the theoretical curve were determined by a biexponential fit of the single-pulse FID. The TQ signals were in close agreement with theory with an absolute deviation of the maximum TQ signals of $<0.42\%$ and a relative deviation of $<1.9\%$ for 2%, 4%, and 6% agar samples. For the 0% agar sample, a non-zero TQ signal was extracted. SP, single pulse.

the weighted sum of the TQ signals of both compartments. The SP TQ signal and expected TQ signal were in close agreement with a maximum deviation of 2.5%.

Figure 6 compares the FIDs and TQ curves with and without noise for different noise levels. Additionally, the noise was subtracted from the TQ signal subsequently to

applying the SP method. Up to a SQ SNR of 10 corresponding to a TQ SNR of 2, the noise-subtracted TQ signal was in close agreement to the TQ signal without noise. The latter can be considered as the ground truth. Even for a SQ SNR of 5 (TQ SNR of 1), the TQ signal only deviated substantially for larger t_{evo} .

TABLE 1 Summary of the fit results for T_2^* and T_2 relaxation times and the amplitudes of the slow and fast component for all agar samples. The 2%, 4%, and 6% agar sample FIDs were fitted using a biexponential fit function and the 0% agar sample using a mono-exponential fit function. The SP FID yielded the T_2^* relaxation times, whereas the TQTPPI FID resulted in the T_2 relaxation times.

Fit results: Relaxation times and amplitudes				
Agar concentration	0%	2%	4%	6%
T_{2s}^* [ms]	19.00 ± 0.09	16.89 ± 0.24	21.26 ± 0.28	17.48 ± 0.13
T_{2f}^* [ms]	-	5.35 ± 0.09	4.65 ± 0.45	3.07 ± 0.32
A_s^*	-	0.42 ± 0.01	0.29 ± 0.01	0.40 ± 0.01
A_f^*	-	0.58 ± 0.01	0.72 ± 0.01	0.60 ± 0.01
T_{2s} [ms]	54.19 ± 0.95	45.03 ± 1.46	39.17 ± 0.73	33.05 ± 0.47
T_{2f} [ms]	-	9.04 ± 0.13	5.12 ± 0.06	3.54 ± 0.04
A_s	-	0.43 ± 0.01	0.42 ± 0.01	0.43 ± 0.01
A_f	-	0.61 ± 0.01	0.62 ± 0.01	0.63 ± 0.01

Abbreviations: FID, free induction decay; SP, single pulse; TQTPPI, triple quantum time proportional phase increment.

TABLE 2 Summary of the sodium TQ/SQ signals for all methods and samples. Additionally, the maximum TQ/SQ signal from the TQTPPI sequence without the 180° refocusing pulse and the mean over the maximum TQ/SQ signals over a single slice for each sample of the imaging phantom are listed (Imaging). For the comparison with the spin echo sequence, the spin echo TQ and the TQTPPI TQ signals were corrected with the T_2 and T_2^* relaxation times, respectively, and with Equation (8).

Maximum TQ/SQ signal [%]				
Agar concentration	0%	2%	4%	6%
SP method	6.04 ± 0.09	11.31 ± 0.34	18.25 ± 0.30	22.67 ± 0.30
Theory	0.00 ± 0.00 ^a	11.16 ± 0.00	18.00 ± 0.00	22.25 ± 0.00
TQTPPI (w 180)	0.04 ± 0.02 ^a	12.46 ± 0.07 ^a	19.84 ± 0.14 ^a	23.93 ± 0.26 ^a
TQTPPI (wo 180)	0.12 ± 0.04 ^a	12.53 ± 0.18 ^a	19.71 ± 0.24 ^a	23.88 ± 0.16 ^a
Imaging	7.31 ± 3.48	13.40 ± 3.65	17.55 ± 3.77	19.77 ± 4.97
Spin echo	0.45 ± 0.60	24.51 ± 0.65	31.05 ± 1.52	32.14 ± 0.73
Theory	0.00 ± 0.00	25.68 ± 0.00	30.98 ± 0.00	32.89 ± 0.00
TQTPPI	0.08 ± 0.04	23.15 ± 0.23	29.94 ± 0.32	34.48 ± 0.46 ^a

Abbreviations: SP, single-pulse; SQ, single quantum.

^aStatistically SD from SP method or spin echo.

3.3 | MR imaging

Combination of a multi-echo version of the UTE sequence and the SP method provided a voxelwise extraction of $SQ(t)$ and $TQ(t)$ relaxation curves for different τ_{evo} . From this data, a SQ image ($\tau_{\text{evo}} = 0$), maximum TQ and sum TQ images were created. Figure 7 shows the SQ, maximum and sum TQ signal images for a sample consisting of agar concentrations of 0%, 2%, 4%, and 6% with 154 mM NaCl. For voxels outside the samples, the noise led to random TQ/SQ values, and consequently values outside the sample were set to 0.

The TQ signal was increasing with agar concentration as demonstrated in Table 2 for the average maximum TQ

signal over one slice for each sample. All voxels, including the edge voxels, were weighted equally. The average value of the maximum TQ signal for the 4% and 6% agar samples were smaller than the values of the SP method, theory, and TQTPPI; however, the 0% and 2% agar values were slightly larger compared to the values of the SP method, theory, and TQTPPI. The uncertainties of the TQ signals were much larger as compared to the single-pulse sequence, and the relative deviations were in the range of 20% to 30%, except for the 0% agar sample where it was around 50%. The relative SD of the SQ image voxels was in the range of 9% to 17%. Similar to the previous spectroscopic NMR measurements, the maximum TQ signal in the MR image was also non-zero for the 0% agar sample.

Comparison of SP method with TQTPPI sequence

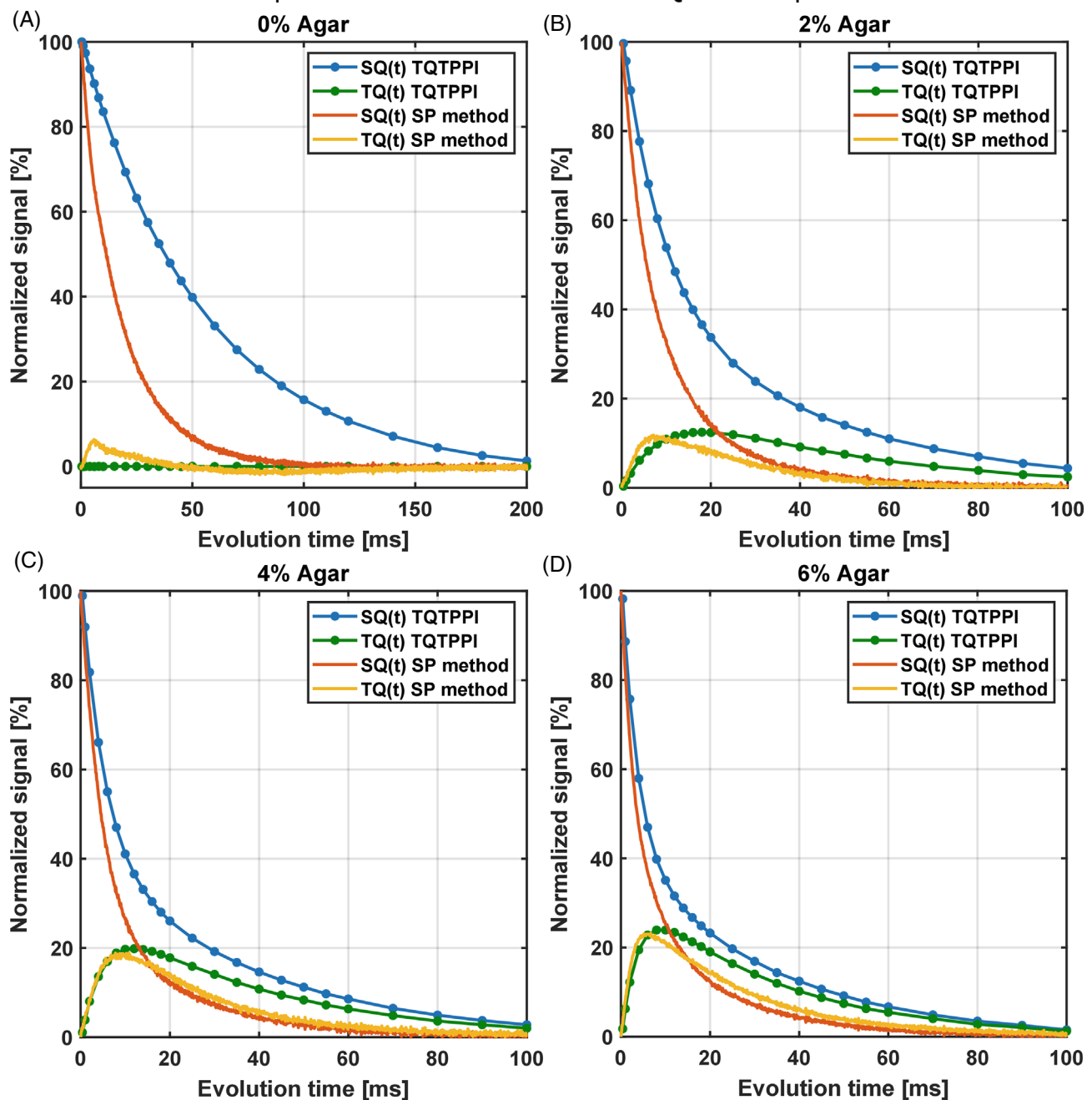


FIGURE 3 Comparison of the SP TQ signal and the TQTPPI sequence with 180° pulse for agar samples with (A) 0%, (B) 2%, (C) 4%, and (D) 6% agar. Because the single-pulse FID decays with T_2^* and the TQTPPI FID with T_2 , the SP extracted TQ signal decayed much faster. For the 2%, 4%, and 6% agar samples, the absolute deviation of the maximum TQ signals was $<1.6\%$ (relative deviation $<9.3\%$). TPPI, time proportional phase increment.

However, in the sum TQ image, the signal of the 0% agar sample was mostly negative or close to 0.

4 | DISCUSSION

The sodium TQ signal promises to be a valuable biomarker for cell viability. Its clinical application has the potential

to boost the value of sodium MRI. However, common TQ techniques require at least three RF pulses and a sophisticated RF pulse phase cycling. Such pulse sequences inherently have a long scan time, increased specific absorption rate, and increased sensitivity to B_0 and B_1 inhomogeneity. Altogether, these major obstacles currently hinder the use of the TQ signal in clinical applications. In this study, a novel way to detect the TQ signal was investigated using

Comparison of TQ signal of spin echo and TQTPPI sequences with theory

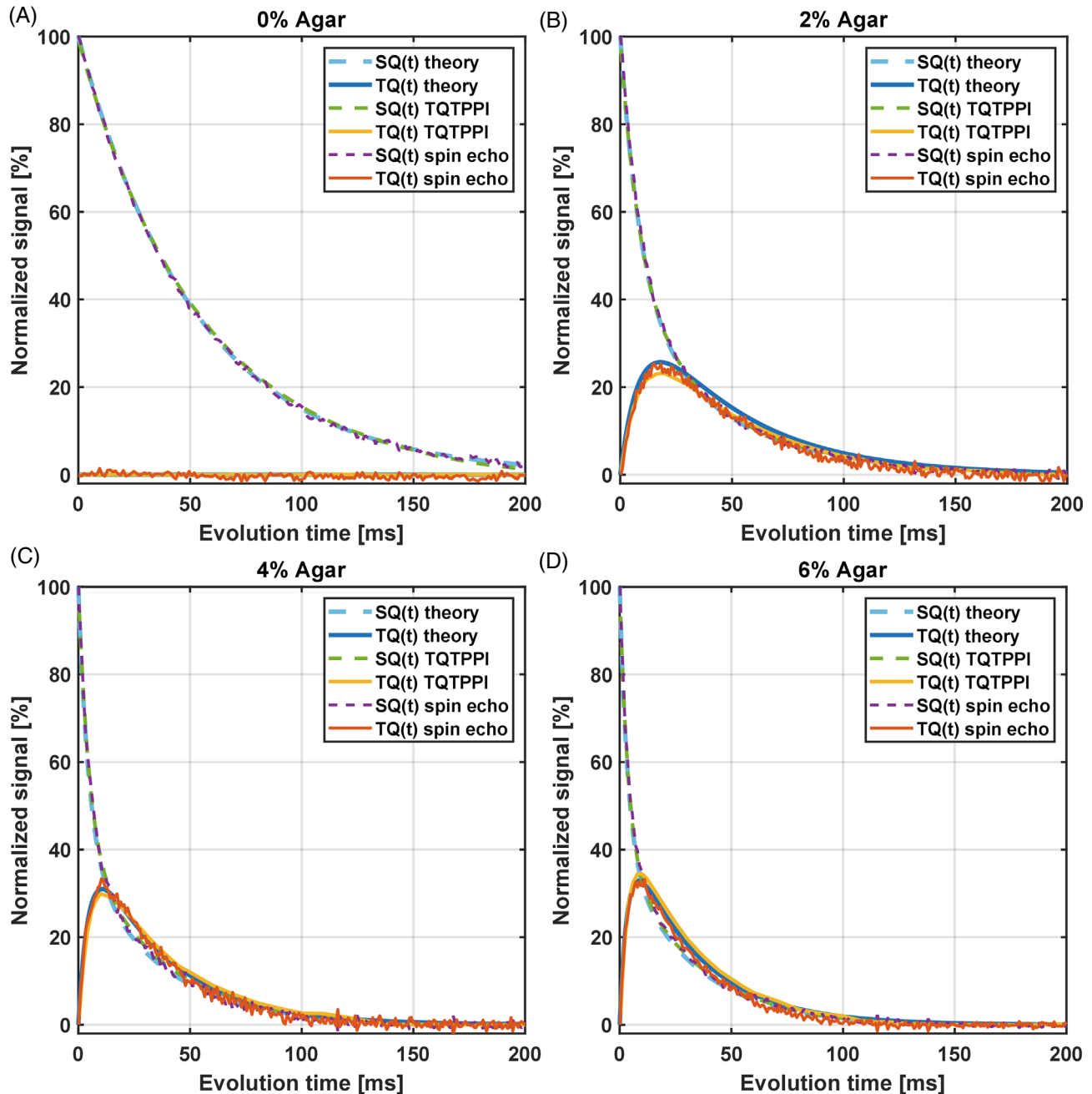


FIGURE 4 Comparison of the TQ signal of the SE sequence, TQTPPI sequence with 180 pulse and the theoretical transfer function $f_{31}^{(1)}(\tau_{\text{evo}})$ for (A) 0%, (B) 2%, (C) 4%, and (D) 6% agar samples. The TQ signals of all methods were in very close agreement. For all samples, the absolute deviations of the maximum TQ signals between SE and theory (TQTPPI) sequence were $<1.2\%$ (2.4%), and relative deviations (0% agar sample excluded) were $<4.6\%$ (6.8%). The SE TQ signal of the 4% agar sample showed an additional increase in the TQ signal around the maximum, which might be an artifact or noise. SE, spin echo.

only a single excitation pulse. Such method allows simultaneous SQ and TQ MR imaging with the same scan time as for the SQ MR image. The approach could be a major step ahead toward the clinical application of TQ imaging.

Comparison of the SP method with theory and the TQTPPI pulse sequence demonstrated the possibility to extract the TQ signal using only a single-pulse sequence.

The extracted TQ signal maxima of the 2%, 4%, and 6% agar samples were in close agreement with theory and TQTPPI experiments. However, the SP FID decays with T_2^* and the TQTPPI FID with the T_2 relaxation times, respectively. Therefore, for a better comparison of the method with the TQTPPI TQ signal, the T_2 FID was additionally sampled using a spin echo sequence followed by application of

Results for MCS with relaxation times for 2% and 6% agar

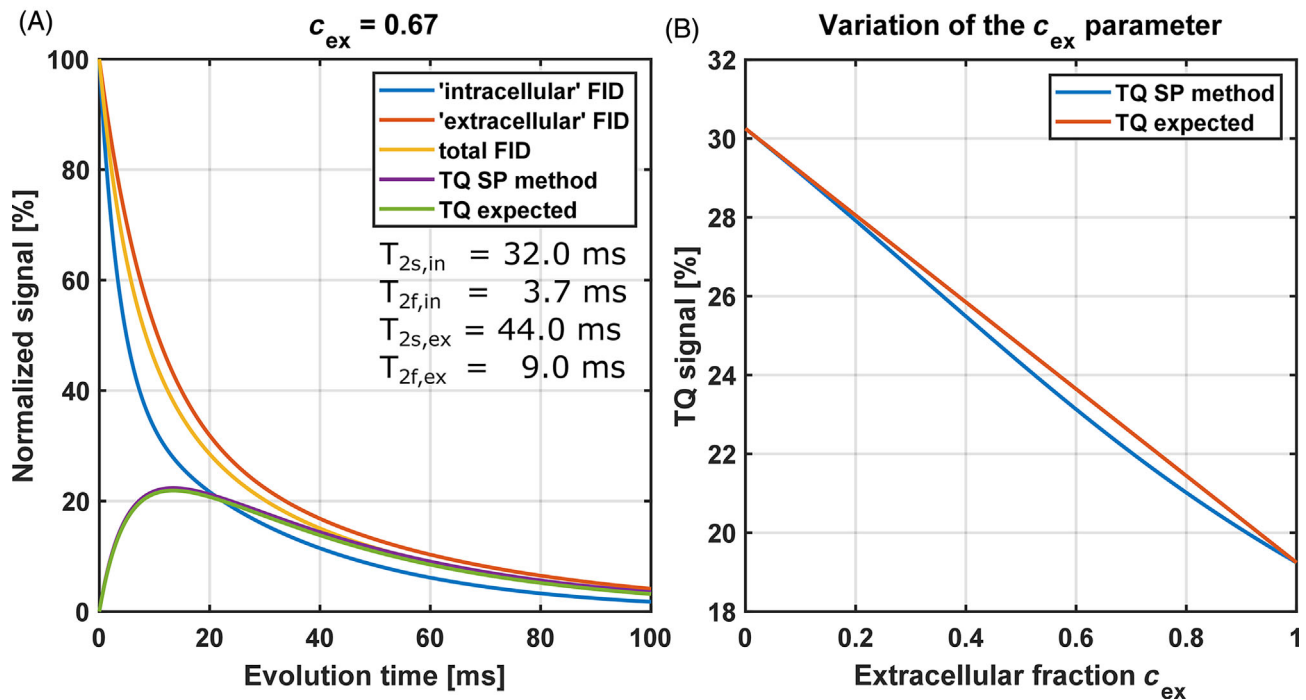


FIGURE 5 Comparison of the TQ signals extracted from the SP method with the expected TQ signal for simulated FIDs of a multi-compartment system with two biexponential compartments. The fraction of the “extracellular” compartment c_{ex} was varied. (A) SQ and TQ signals for $c_{ex} = 0.67$, the value with the maximum deviation of the TQ maximum between the SP method TQ signal, and the expected TQ signal. (B) Maximum SP method and expected TQ signals in dependence of c_{ex} . The SP method is in close agreement with the expected TQ signal for all c_{ex} values with a maximum deviation of 2.5%.

the SP method. This comparison also showed a very close agreement between the SP method of the SE FID, TQTPPI sequence, and theoretical prediction for these samples. This demonstrated that the application of SP method is not limited to SP sequences. Nevertheless, the 0% agar sample yielded a non-zero TQ signal using the SP method of the SP FID, whereas it vanished for the SE FID. The non-zero TQ signal of the SP FID did not result in the typical “buildup” behavior of the TQ signal. This cannot be explained by a multi-compartment model and indicates that the shape of the FID was nonexponential. This might be caused by non-Lorentzian-distributed B_0 inhomogeneities. For example, Steidle and Schick⁶⁷ reported a Gaussian component in the intravoxel distribution of B_0 inhomogeneities for ^1H scans. Another possible explanation for the nonexponential decay might be a hardware artifact. The Gibbs-like artifact described in the Supporting Information was caused by the impulse response of digital filters,⁶⁸ which might also introduce additional imperfections. Measurements on other MRI systems are necessary to further investigate the origin of the nonexponential behavior in the SP FID.

The non-zero TQ signal of 0% agar sample may be an indication of the influence of B_0 inhomogeneity on the TQ

signal. For example, non-Lorentzian distributed B_0 inhomogeneities with a nonexponential T_2^* decay can lead to a contribution to the TQ signal that does not originate from T_{31} coherences. The influence on the TQ signal of the 2%, 4%, and 6% agar samples may be reduced due to a short T_{2f} component. The impact of B_0 inhomogeneity on the conventional TQ multi-pulse sequences is more complicated because each coherence order is influenced differently. There exist different approaches to minimize the effect of B_0 inhomogeneity on the signal, for example, by adapting the phase cycle.^{29,30,47,49,51} Another approach is to use a 180° refocusing pulse, which refocuses the signal such that T_2 instead of T_2^* relaxation times determine the signal.⁶ However, this approach requires an accurate calibration of the 180° pulse. In summary, both methods to measure the TQ signal are affected by B_0 inhomogeneity in a different way.

In contrast to B_0 inhomogeneity, the flip angle, that is, B_1 inhomogeneity, only determines the overall SQ signal using the SP method. Thus, it changes the absolute signal value but not the relative TQ/SQ signal. However, the conventional TQ pulse sequences are very sensitive to imperfect pulses; for example, the TQ signal depends with $\sin^5(\theta)$ on the flip angle θ .⁵¹ Thus, small imperfections in

Impact of noise on the estimation of the SP TQ signal

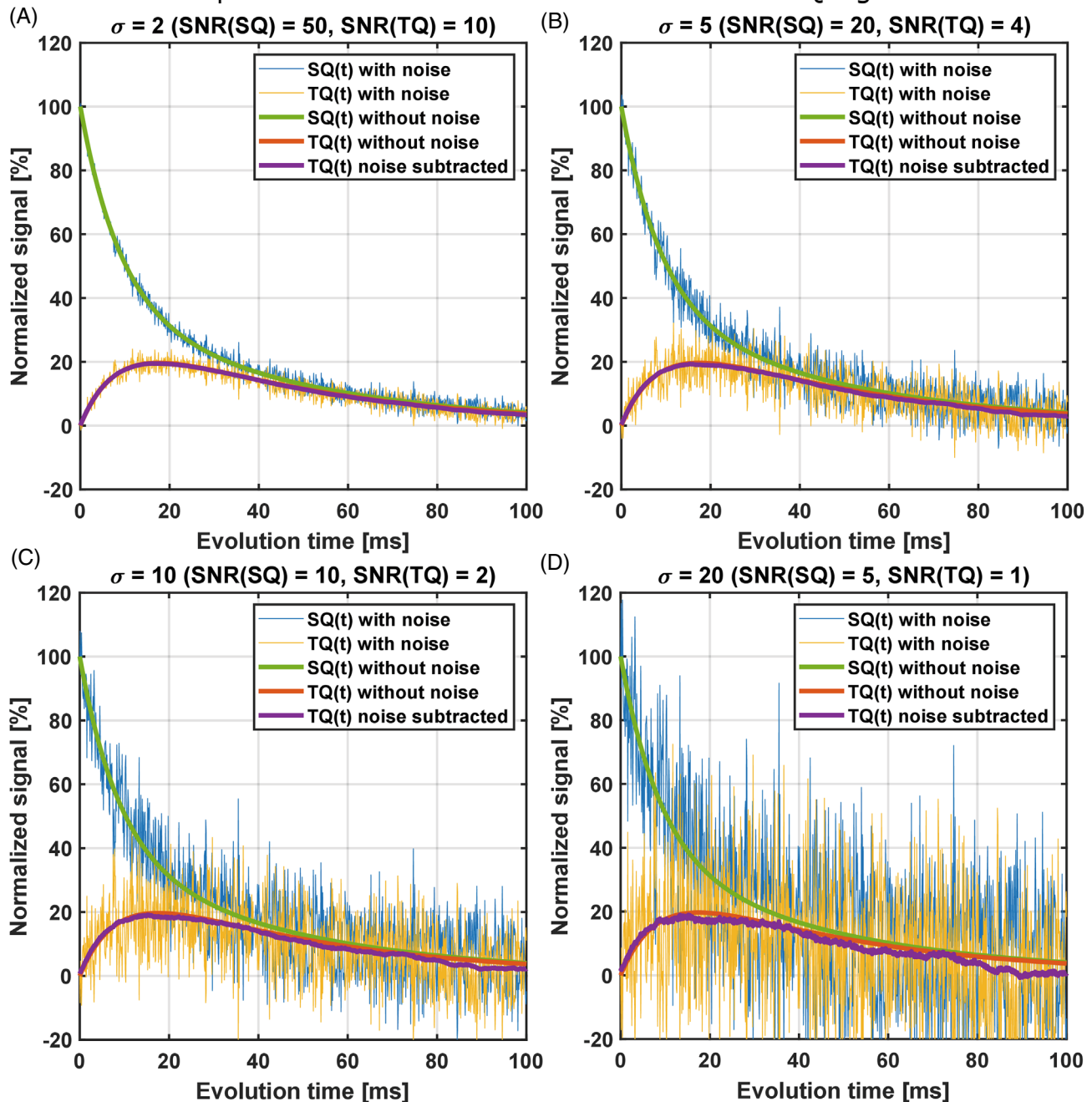


FIGURE 6 Comparison of the impact of different noise levels on the accuracy of the extracted TQ signal determined with the SP method. σ is the SD of the Gaussian noise. The TQ signal without noise is shown in red. The purple curve shows the SP TQ signal of the noisy FID with the same noise subtracted subsequently. This curve shows the systematic error of the SP method. Even for high noise levels, that is, SQ SNR = 5, the systematic error on the TQ signal was small for evolution times in the range of the maximum TQ signal. The absolute deviation of the maximum TQ signal $<0.7\%$ and relative deviation $\sim 3.6\%$ for $\sigma = 20$, respectively.

the calibration or an inhomogeneous RF excitation have severe effects on the TQ signal.⁵¹ In summary, the SP method is less prone to B_1 inhomogeneities compared to conventional TQ pulse sequences.

The in vivo situation is more complex and closer to a multi-compartment system. In this case, the integrals in Equation (7) become more complicated, and the difference

between both terms does not exactly equal the TQ signal anymore. We used a two-compartment system with two biexponential compartments to simulate the in vivo situation. The TQ signal was systematically slightly overestimated by the SP method. However, the deviation to the expected TQ signal was $<2.5\%$ for the case of biexponential relaxation in both compartments. Hence, the

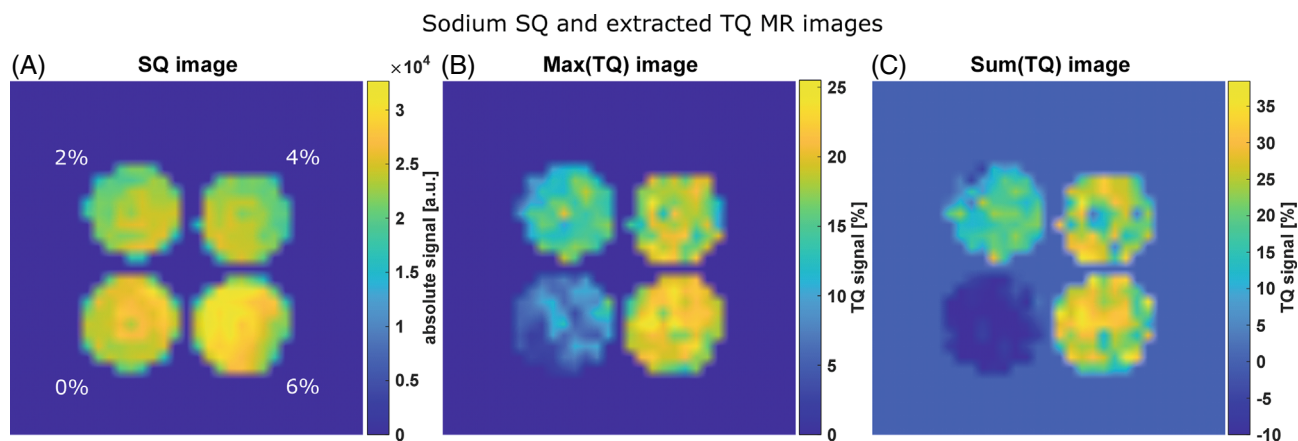


FIGURE 7 Sodium SQ and extracted TQ MR images from the agarose samples. (A) SQ signal using minimum τ_{evo} 3 and 4. (B) Maximum of the extracted TQ signal. The extracted TQ signal was increasing with agar concentration. The 0% agar sample yielded a non-zero TQ signal as demonstrated on Fig. 3 and Fig. 4. (C) Sum of the extracted TQ signal normalized by the sum of the SQ signal. For the 0% agar sample, the sum of the extracted TQ signals was negative, which resulted from the untypical extracted TQ evolution curve. The color bar range was limited to -10% to increase visibility.

SP method is also applicable to more complicated in vivo situations.

One drawback of this method arises in the case of two mono-exponential compartments. This case cannot be distinguished mathematically from the case of one biexponential compartment, and the SP “TQ” signal is the same in both cases. In contrast, the TQTPPI TQ signal is vanishing for the case of two mono-exponential compartments. In our experiment, a similar situation occurred for the 0% agar sample. Here, the FID did not decay mono-exponentially; consequently, the SP “TQ” signal was not zero compared to the TQTPPI sequence. Furthermore, the “TQ” signal also contains the T_{21} double quantum signal in a macroscopically anisotropic environment. Therefore, we may call the SP extracted “TQ” signal a measure of the “deviation from mono-exponential decay.” However, the main source for biexponential decay is the quadrupole interaction. Furthermore, the signal in the multi-compartment case was in close agreement to the TQ signal and showed the expected behavior for the increase of the TQ signal. Therefore, the extracted TQ signal of this method approximates the usually observed TQ signal.

The SP method is attractive not only for spectroscopy but in particular for the fast estimation of the TQ signal in MR imaging. The method approximates the TQ signal in a single shot with the high time efficiency of the SQ signal. This means that, without increasing scan time, both SQ and TQ images can be acquired instead of only an SQ image. As a proof-of-concept, we used a 3D UTE sequence with multiple echoes to sample the complete FID in one shot. Because TR is usually set to $3 \cdot T_1$ to $5 \cdot T_1$, there

is plenty of time to sample the entire FID with only one excitation. Furthermore, the SP method samples the entire TQ evolution curve instead of the TQ signal at a specific evolution time τ_{evo} . Hence, the maximum TQ signal of different tissues with different optimum evolution times can be obtained within a single measurement.

The TQ signals of a single slice were smaller with larger uncertainties than the spectroscopic sequences. Partial volume effects and a large noise level influence the TQ signals. Our current pulse sequence was not optimized for sodium MR imaging and was only used as a proof of concept. Both the sequence parameters as well as the image reconstruction method can be further improved, for example, by optimizing the bandwidth, correct for imperfections in the k-space trajectories, etc.^{65,69–71} Alternatively, the SP method can also simply be applied to the processing pipeline of existing sodium multi-echo imaging protocols^{71–73} to acquire the TQ signal additionally without increasing overall scan time.

In preparation for the imaging sequence, the impact of noise on the accuracy of the SP method was investigated with simulated data. Even for low SNRs, that is, SQ SNR < 10 , the impact of the SP method on the TQ signal was small for the relevant evolution times around the TQ maximum with an absolute deviation of $< 0.7\%$ and a relative deviation of $< 4\%$. Typical sodium MRI SNR values are equal or larger than 10.^{71,74} However, because the TQ signal in tissue is around 10% of the SQ signal, longer scan times to increase SNR might still be necessary. The SP method performed well in low SNR scenarios and was only limited by the fact that the TQ signal is smaller than the SQ signal.

5 | CONCLUSION

A novel method to extract the sodium TQ signal using a single-pulse sequence was proposed. This method allows a simultaneous acquisition of SQ and TQ signals without extra RF pulses and extensive phase cycling. The extracted TQ signal was in close agreement with theory and the results of TQTPPI sequence. In multi-compartment systems and for noisy data, the extracted TQ signal reproduced the expected TQ signal behavior. This approach combined with multi-echo UTE imaging represents an efficient method to extract the TQ signal in vivo. This approach may expand TQ imaging applications and thus may leverage the full potential of TQ signal.

ACKNOWLEDGEMENTS

A portion of this work was performed at the National High Magnetic Field Laboratory, which is supported by the National Science Foundation (NSF) Cooperative Agreement, number DMR-1644779, and the State of Florida. Part of this work was supported by the German Research Foundation (DFG), grant no. 410981386. Open Access funding enabled and organized by Projekt DEAL.

ORCID

Simon Reichert  <https://orcid.org/0000-0002-6013-8242>

Victor Schepkin  <https://orcid.org/0000-0001-5475-2636>

Frank G. Zöllner  <https://orcid.org/0000-0003-3405-1394>

REFERENCES

- Hu R, Kleimaier D, Malzacher M, Hoesl MAU, Paschke NK, Schad LR. X-nuclei imaging: current state, technical challenges, and future directions. *J Magn Reson Imaging*. 2020;51:355-376.
- Thulborn KR. Quantitative sodium MR imaging: a review of its evolving role in medicine. *Neuroimage*. 2018;168:250-268.
- Madelin G, Lee J-S, Regatte RR, Jerschow A. Sodium MRI: methods and applications. *Prog Nucl Magn Reson Spectrosc*. 2014;79:14-47.
- Alberts B. Molecular biology of the cell 5E. *Garland Sci*. 2008;2008:1121-1128.
- Clausen MV, Hilbers F, Poulsen H. The structure and function of the Na,K-ATPase isoforms in health and disease. *Front Physiol*. 2017;8:371.
- Schepkin VD, Neubauer A, Nagel AM, Budinger TF. Comparison of potassium and sodium binding in vivo and in agarose samples using TQTPPI pulse sequence. *J Magn Reson*. 2017;277:162-168.
- Schepkin VD. Statistical tensor analysis of the MQ MR signals generated by weak quadrupole interactions. *Zeitschrift für Medizinische Physik*. 2019;29:326-336.
- Rooney WD, Springer CS. A comprehensive approach to the analysis and interpretation of the resonances of spins 3/2 from living systems. *NMR Biomed*. 1991;4:209-226.
- Rooney WD, Springer CS Jr. The molecular environment of intracellular sodium: ^{23}Na NMR relaxation. *NMR Biomed*. 1991;4:227-245.
- van der Maarel JRC. Thermal relaxation and coherence dynamics of spin 3/2. I. Static and fluctuating quadrupolar interactions in the multipole basis. *Concepts Magn Reson Part A*. 2003;19A:97-116.
- van der Maarel JRC. Thermal relaxation and coherence dynamics of spin 3/2. II. Strong radio-frequency field. *Concepts Magn Reson Part A*. 2003;19A:117-133.
- Lachner S, Ruck L, Niesporek SC, et al. Comparison of optimized intensity correction methods for ^{23}Na MRI of the human brain using a 32-channel phased array coil at 7 Tesla. *Zeitschrift für Medizinische Physik*. 2020;30:104-115.
- Malzacher M, Chacon-Caldera J, Paschke N, Schad LR. Feasibility study of a double resonant ($^1\text{H}/^{23}\text{Na}$) abdominal RF setup at 3T. *Zeitschrift für Medizinische Physik*. 2019;29:359-367.
- Rooney WD, Li X, Sammi MK, Bourdette DN, Neuwelt EA, Springer CS Jr. Mapping human brain capillary water lifetime: high-resolution metabolic neuroimaging. *NMR Biomed*. 2015;28:607-623.
- Dizon JM, Tauskela JS, Wise D, Burkhoff D, Cannon PJ, Katz J. Evaluation of triple-quantum-filtered ^{23}Na NMR in monitoring of intracellular na content in the perfused rat heart: comparison of intra- and extracellular transverse relaxation and spectral amplitudes. *Magn Reson Med*. 1996;35:336-345.
- Eykyn TR, Aksentijević D, Aughton KL, Southworth R, Fuller W, Shattock MJ. Multiple quantum filtered ^{23}Na NMR in the Langendorff perfused mouse heart: ratio of triple/double quantum filtered signals correlates with [Na]i. *J Mol Cell Cardiol*. 2015;86:95-101.
- Jelicks LA, Gupta RK. On the extracellular contribution to multiple quantum filtered ^{23}Na NMR of perfused rat heart. *Magn Reson Med*. 1993;29:130-133.
- Knubovets T, Shinar H, Navon G. Quantification of the contribution of extracellular sodium to ^{23}Na multiple-quantum-filtered NMR spectra of suspensions of human red blood cells. *J Magn Reson*. 1998;131:92-96.
- Schepkin VD, Choy IO, Budinger TF. Sodium alterations in isolated rat heart during cardioplegic arrest. *J Appl Physiol*. 1996;81:2696-2702.
- Schepkin VD, Choy IO, Budinger TF, et al. Sodium TQF NMR and intracellular sodium in isolated crystalloid perfused rat heart. *Magn Reson Med*. 1998;39:557-563.
- Seshan V, Sherry AD, Bansal N. Evaluation of triple quantum-filtered ^{23}Na NMR spectroscopy in the in situ rat liver. *Magn Reson Med*. 1997;38:821-827.
- Winter PM, Bansal N. Triple-quantum-filtered ^{23}Na NMR spectroscopy of subcutaneously implanted 9L gliosarcoma in the rat in the presence of TmDOTP(5 - 1). *J Magn Reson*. 2001;152:70-78.
- Neumaier-Probst E, Konstandin S, Ssozi J, et al. A double-tuned $^1\text{H}/^{23}\text{Na}$ resonator allows 1H-guided ^{23}Na -MRI in ischemic stroke patients in one session. *Int J Stroke*. 2015;10:56-61.
- Ouwerkerk R, Bleich KB, Gillen JS, Pomper MG, Bottomley PA. Tissue sodium concentration in human brain tumors as measured with ^{23}Na MR imaging. *Radiology*. 2003;227:529-537.
- Schepkin VD, Chenevert TL, Kuszpit K, et al. Sodium and proton diffusion MRI as biomarkers for early therapeutic response in subcutaneous tumors. *Magn Reson Imaging*. 2006;24:273-278.

26. Schepkin VD, Lee KC, Kuszpit K, et al. Proton and sodium MRI assessment of emerging tumor chemotherapeutic resistance. *NMR Biomed.* 2006;19:1035-1042.
27. Schepkin VD, Ross BD, Chenevert TL, et al. Sodium magnetic resonance imaging of chemotherapeutic response in a rat glioma. *Magn Reson Med.* 2005;53:85-92.
28. Zaric O, Pinker K, Zbyn S, et al. Quantitative sodium MR imaging at 7 T: initial results and comparison with diffusion-weighted imaging in patients with breast tumors. *Radiology.* 2016;280:39-48.
29. Fiege DP, Romanzetti S, Mirkes CC, Brenner D, Shah NJ. Simultaneous single-quantum and triple-quantum-filtered MRI of ^{23}Na (SISTINA). *Magn Reson Med.* 2013;69:1691-1696.
30. Hoesl MAU, Schad LR, Rapacchi S. Efficient ^{23}Na triple-quantum signal imaging on clinical scanners: cartesian imaging of single and triple-quantum ^{23}Na (CRISTINA). *Magn Reson Med.* 2020;84:2412-2428.
31. Worthoff WA, Shymanskaya A, Shah NJ. Relaxometry and quantification in simultaneously acquired single and triple quantum filtered sodium MRI. *Magn Reson Med.* 2019;81:303-315.
32. Choy IO, Schepkin VD, Budinger TF, Obayashi DY, Young JN, DeCampi WM. Effects of specific sodium/hydrogen exchange inhibitor during cardioplegic arrest. *Ann Thorac Surg.* 1997;64:94-99.
33. Schepkin VD, Choy IO, Budinger TF, Young JN, DeCampi WM. Multi-dose crystalloid cardioplegia preserves intracellular sodium homeostasis in myocardium. *J Mol Cell Cardiol.* 1999;31:1643-1651.
34. Tauskela JS, Dizon JM, Whang J, Katz J. Evaluation of multiple-quantum-filtered ^{23}Na NMR in monitoring intracellular Na content in the isolated perfused rat heart in the absence of a chemical-shift reagent. *J Magn Reson.* 1997;127:115-127.
35. LaVerde G, Nemoto E, Jungreis CA, Tanase C, Boada FE. Serial triple quantum sodium MRI during non-human primate focal brain ischemia. *Magn Reson Med.* 2007;57:201-205.
36. Babsky AM, Zhang H, Hekmatyar SK, Hutchins GD, Bansal N. Monitoring chemotherapeutic response in RIF-1 tumors by single-quantum and triple-quantum-filtered ^{23}Na MRI, ^1H diffusion-weighted MRI and PET imaging. *Magn Reson Imaging.* 2007;25:1015-1023.
37. Winter PM, Poptani H, Bansal N. Effects of chemotherapy by 1,3-Bis(2-chloroethyl)-1-nitrosourea on single-quantum- and triple-quantum-filtered ^{23}Na and ^{31}P nuclear magnetic resonance of the subcutaneously implanted 9L glioma. *Cancer Res.* 2001;61:2002-2007.
38. Gottwald E, Kleintschek T, Giselbrecht S, et al. Characterization of a chip-based bioreactor for three-dimensional cell cultivation via Magnetic Resonance Imaging. *Zeitschrift für Medizinische Physik.* 2013;23:102-110.
39. Hoesl MAU, Kleimaier D, Hu R, et al. ^{23}Na Triple-quantum signal of in vitro human liver cells, liposomes, and nanoparticles: cell viability assessment vs. separation of intra- and extracellular signal. *J Magn Reson Imaging.* 2019;50:435-444.
40. Kleimaier D, Schepkin V, Nies C, Gottwald E, Schad LR. Intracellular sodium changes in cancer cells using a microcavity array-based bioreactor system and sodium triple-quantum MR signal. *Processes.* 2020;8:1267.
41. Neubauer A, Nies C, Schepkin VD, et al. Tracking protein function with sodium multi quantum spectroscopy in a 3D-tissue culture based on microcavity arrays. *Sci Rep.* 2017;7:3943.
42. Kleimaier D, Schepkin V, Hu R, Schad LR. Protein conformational changes affect the sodium triple-quantum MR signal. *NMR Biomed.* 2020;33:e4367.
43. Bodenhausen G. Multiple-quantum NMR. *Prog Nucl Magn Reson Spectrosc.* 1980;14:137-173.
44. Chung C-W, Wimperis S. Optimum detection of spin-32 biexponential relaxation using multiple-quantum filtration techniques. *J Magn Reson.* 1990;88:440-447.
45. Jaccard G, Wimperis S, Bodenhausen G. Multiple-quantum NMR spectroscopy of $S=3/2$ spins in isotropic phase: a new probe for multiexponential relaxation. *J Chem Phys.* 1986;85:6282-6293.
46. Navon G, Shinar H, Eliav U, Seo Y. Multiquantum filters and order in tissues. *NMR Biomed.* 2001;14:112-132.
47. Fleysher L, Oesingmann N, Inglese M. B_0 inhomogeneity-insensitive triple-quantum-filtered sodium imaging using a 12-step phase-cycling scheme. *NMR Biomed.* 2010;23:1191-1198.
48. Reddy R, Shinnar M, Wang Z, Leigh JS. Multiple-quantum filters of spin-32 with pulses of arbitrary flip angle. *J Magn Reson, Series B.* 1994;104:148-152.
49. Tanase C, Boada FE. Triple-quantum-filtered imaging of sodium in presence of B_0 inhomogeneities. *J Magn Reson.* 2005;174:270-278.
50. Rance M, Sørensen OW, Bodenhausen G, Wagner G, Ernst RR, Wüthrich K. Improved spectral resolution in COSY ^1H NMR spectra of proteins via double quantum filtering. *Biochem Biophys Res Commun.* 1983;117:479-485.
51. Hancu I, Boada FE, Shen GX. Three-dimensional triple-quantum-filtered ^{23}Na imaging of in vivo human brain. *Magn Reson Med.* 1999;42:1146-1154.
52. Hancu I, van der Maarel JRC, Boada FE. A model for the dynamics of spins $3/2$ in biological media: signal loss during radiofrequency excitation in triple-quantum-filtered sodium MRI. *J Magn Reson.* 2000;147:179-191.
53. Fano U, Racah G. *Irreducible Tensorial Sets.* Vol 4. Academic Press; 1959.
54. Gast LV, Gerhalter T, Hensel B, Uder M, Nagel AM. Double quantum filtered ^{23}Na MRI with magic angle excitation of human skeletal muscle in the presence of B_0 and B_1 inhomogeneities. *NMR Biomed.* 2018;31:e4010.
55. Stobbe RW, Beaulieu C. Residual quadrupole interaction in brain and its effect on quantitative sodium imaging. *NMR Biomed.* 2016;29:119-128.
56. Tsang A, Stobbe RW, Beaulieu C. In vivo double quantum filtered sodium magnetic resonance imaging of human brain. *Magn Reson Med.* 2015;73:497-504.
57. Foy BD, Burstein D. Interstitial sodium nuclear magnetic resonance relaxation times in perfused hearts. *Biophys J.* 1990;58:127-134.
58. Gilles A, Nagel AM, Madelin G. Multipulse sodium magnetic resonance imaging for multicompartiment quantification: proof-of-concept. *Sci Rep.* 2017;7:17435.
59. Pettegrew JW, Woessner DE, Minshew NJ, Glonek T. Sodium- ^{23}Na NMR analysis of human whole blood, erythrocytes, and plasma. Chemical shift, spin relaxation, and intracellular sodium concentration studies. *J Magn Reson.* 1984;57:185-196.
60. Shinar E, Rachmilewitz EA, Shifter A, Rahamin E, Saltman P. Oxidative damage to human red cells induced by copper and

- iron complexes in the presence of ascorbate. *Biochim Biophys Acta Mol Cell Res.* 1989;1014:66-72.
61. Shinar H, Navon G. Sodium-23 NMR relaxation times in nucleated red blood cells and suspensions of nuclei. *Biophys J.* 1991;59:203-208.
 62. Winter PM, Bansal N. TmDOTP5- as a ^{23}Na shift reagent for the subcutaneously implanted 9L gliosarcoma in rats. *Magn Reson Med.* 2001;45:436-442.
 63. Konstandin S, Krämer P, Günther M, Schad LR. Sodium magnetic resonance imaging using ultra-short echo time sequences with anisotropic resolution and uniform k-space sampling. *Magn Reson Imag.* 2015;33:319-327.
 64. Kullberg J, Ahlström H, Johansson L, Frimmel H. Automated and reproducible segmentation of visceral and subcutaneous adipose tissue from abdominal MRI. *Int J Obes.* 2007;31:1806-1817.
 65. Licht C, Reichert S, Guye M, Schad LR, Rapacchi S. Multidimensional compressed sensing to advance ^{23}Na multi-quantum coherences MRI. *Magn Reson Med.* 2024;91:926-941.
 66. Ozdemir S, Ider YZ. bSSFP phase correction and its use in magnetic resonance electrical properties tomography. *Magn Reson Med.* 2019;81:934-946.
 67. Steidle G, Schick F. A new concept for improved quantitative analysis of reversible transverse relaxation in tissues with variable microscopic field distribution. *Magn Reson Med.* 2021;85:1493-1506.
 68. Moskau D. Application of real time digital filters in NMR spectroscopy. *Concepts Magn Reson.* 2002;15:164-176.
 69. Adlung A, Licht C, Reichert S, et al. Quantification of tissue sodium concentration in the ischemic stroke: a comparison between external and internal references for ^{23}Na MRI. *J Neurosci Methods.* 2022;382:109721.
 70. Adlung A, Paschke NK, Golla A-K, et al. ^{23}Na MRI in ischemic stroke: acquisition time reduction using postprocessing with convolutional neural networks. *NMR Biomed.* 2021;34:e4474.
 71. Blunck Y, Josan S, Taqdees SW, et al. 3D-multi-echo radial imaging of ^{23}Na (3D-MERINA) for time-efficient multi-parameter tissue compartment mapping. *Magn Reson Med.* 2018;79:1950-1961.
 72. Alhulail AA, Xia P, Shen X, et al. Fast in vivo ^{23}Na imaging and mapping using accelerated 2D-FID UTE magnetic resonance spectroscopic imaging at 3 T: proof of concept and reliability study. *Magn Reson Med.* 2021;85:1783-1794.
 73. Syeda W, Blunck Y, Kolbe S, Cleary JO, Johnston LA. A continuum of components: flexible fast fraction mapping in sodium MRI. *Magn Reson Med.* 2019;81:3854-3864.
 74. Nagel AM, Laun FB, Weber M-A, Matthies C, Semmler W, Schad LR. Sodium MRI using a density-adapted 3D radial acquisition technique. *Magn Reson Med.* 2009;62:1565-1573.

SUPPORTING INFORMATION

Additional supporting information may be found in the online version of the article at the publisher's website.

Figure S1. Schematic overview of the single-pulse FID pre-processing. (A) The Gibbs-like artifact was removed by inverting the left part of the first dashed red line to the free induction decay (FID). (b) Zoomed area of the corrected Gibbs artifact. To remove the non-exponential part of the FID, the FID was cut at the second dashed red line which is defined as $t = 0$ ms. This removed 1 ms of the FID. (c) Final post-processed FID for 0% agar.

Figure S2. First dimension free induction decay (FID) of the TQTPPI sequence without the 180° refocusing pulse using the 0% agar sample and an evolution time of 30 ms. The second and third 90° pulses effectively acted like an 180° pulse, leading to a signal echo. Since the TQTPPI FID was created using the integral over the first dimension FIDs, this led to relaxation times not equal to T_2 or T_2^* .

Figure S3. Comparison of the SP TQ signal and the TQTPPI sequence (without 180° refocusing pulse) for agar samples with (A) 0%, (B) 2%, (C) 4% and (D) 6% agar. The TQTPPI FID was biased by echoes in the first dimension FIDs (Figure S2). The resulting TQTPPI FID did neither decay with T_2 nor T_2^* relaxation times.

How to cite this article: Reichert S, Schepkin V, Kleimaier D, Zöllner FG, Schad LR. Sodium triple quantum MR signal extraction using a single-pulse sequence with single quantum time efficiency. *Magn Reson Med.* 2024;92:900-915. doi: 10.1002/mrm.30107